Experimental determination of gold speciation in sulfide-rich hydrothermal fluids from reduced to oxidized

Trigub, A. L.; Tagirov, B. R.; Kvashnina, K. O.; Lafuerza, S.; Filmonova, O. N.; Nickolsky, M. S.;

Originally published:

September 2017

Chemical Geology 471(2017), 52-64

DOI: https://doi.org/10.1016/j.chemgeo.2017.09.010

EXPERIMENTAL DETERMINATION OF GOLD SPECIATION IN SULFIDE-RICH HYDROTHERMAL FLUIDS FROM REDUCED TO OXIDIZED

A.L. Trigub[1,2,5], B.R. Tagirov[1]*, K.O. Kvashnina[3,4], S. Lafuerza[3], O.N. Filmonova[1], M.S. Nickolsky[1]

[1] Institute of Geology of Ore Deposits (IGEM RAS), 35, Staromonetnyi per., 119017 Moscow, Russia

[2] National Research Centre 'Kurchatov Institute', 1 Akademika Kurchatova pl., 123182 Moscow, Russisa

[3] ESRF - The European Synchrotron, CS40220, 38043 Grenoble Cedex 9, France

[4] Helmholtz-Zentrum Dresden-Rossendorf (HZDR), Institute of Resource Ecology, P.O. Box 510119, 01314, Dresden, Germany

[5] Physico-Technical Institute of UB RAS, Kirova st. 132, 426000 Izhevsk, Russia

***Corresponding author:** e-mail tagir@igem.ru, phone +7-499-2308231

To be submitted to Chemical Geology, May 2017

ABSTRACT

The oxidation state of hydrothermal fluids, which form economic deposits of noble metals, varies in wide limits – from oxidized ones typical for porphyry mineralization to reduced which formed volcanogenic massive sulfide deposits. Sulfur-bearing species, along with chloride, are the most important ligands that form stable aqueous complexes with Au and determine Au concentration in natural ore-generating fluids. Depending on the $f(O_2)$ value, in high-temperature fluids (t > 300 °C) the dominant forms of sulfur are sulfides (H_2S, HS^-), sulfites (SO_2, HSO_3^-, SO_3^{2-}), sulfates (HSO_4^-, SO_4^{2-}), and the radical species (S_3^-). Here we report an investigation of Au complexation in high-temperature sulfide-bearing fluids of contrasting oxidation states. The solubility of Au was measured in "oxidized" sulfide fluid (H_2S/SO_4^{2-} buffer controls the *Red/Ox* state) at 450 °C, 1000 bar, and compared with the Au solubility in "reduced" sulfide systems (H_2S/HS^- predominate) reported in the literature. The measured values of the Au solubility matches best the model of the formation of $Au(HS)_2^-$ at near-neutral to weakly acidic pH, and AuHS° in acidic solutions. The solubility constants have been determined for the reactions,

$$Au_{(cr)} + H_2S°_{(aq)} + HS^- = Au(HS)_2^- + 0.5\ H_{2(g)} \qquad \log K_{Au(HS)_2^-} = -0.9 \pm 0.1 \quad ,$$

$$Au_{(cr)} + H_2S°_{(aq)} = AuHS°_{(aq)} + 0.5\ H_{2(g)} \qquad \log K_{AuHS} = -6.5 \pm 0.1 \quad .$$

The average value of $\log K_{Au(HS)_2^-} = -1.3 \pm 0.5$ was calculated for 450 °C (P = 500 – 1500 bar) using all the available Au solubility constants obtained in both "reduced" and "oxidized" sulfide systems. The local atomic environment of Au in high-temperature hydrothermal fluids has been studied using X-ray absorption fine structure spectroscopy (XAFS) in high energy resolution fluorescence detection (HERFD) mode in combination with *ab initio* molecular dynamics (AIMD) and Reverse Monte Carlo (RMC) simulations. Interpretation of Au L_3-edge EXAFS spectra showed that, independently of the *Red*/*Ox* (sulfide or sulfide/sulfate systems) and *PT* – conditions (350 – 450 °C, 500 bar) two S atoms are located in the first coordination shell of Au at 2.29±0.02Å. Comparison of the experimental spectra with those simulated by means of AIMD revealed that EXAFS spectroscopy is not sensitive to the presence of light atoms like S in a distant coordination shell of

Au. However, theoretical calculations indicated that the shape of Au L_3-edge HERFD-XANES spectra depends upon the composition of the distant coordination shell and, therefore, can be used to discriminate between $Au(HS)_2^-$, Au-(HS)-S_3^- and, probably, other complexes with distant-coordination-shell anions. Experimental Au L_3-edge HERFD-XANES spectra are identical for all studied *PT*- and *Red/Ox*-parameters. These results allowed us to conclude that $Au(HS)_2^-$ complex predominates Au speciation in weakly acidic to weakly alkaline pH independently from the oxidation state of the fluid. Besides that, XAFS experiment demonstrated that the formation of mixed Au-HS-Cl complex can be neglected. With increasing pressure (to *n*·kbar) or decreasing temperature (to < 300 °C), due to increasing of concentration of S species in intermediate oxidation states, formation of the Au-HS complexes can be accompanied by the formation of other species with (hydro)sulfite, thiosulfate, (hydro)polysulfide, and sulfur radicals, which would enhance the hydrothermal Au mobility. Stability of these complexes needs further experimental and theoretical examination.

Key words: gold, solubility, hydrothermal fluids, hydrosulfide complexes, stability constants, X-ray absorption spectroscopy, HERFD-XAS, *ab initio* molecular dynamics

1. Introduction

It is generally accepted that Au is transported by natural ore-forming fluids in the form of hydrosulfide or chloride species. Depending on HS^- and Cl^- activity, $AuCl_2^-$, $Au(HS)_2^-$, or AuHS° complexes predominate Au speciation (e.g., Seward, 1973; Zotov et al., 1991; Benning and Seward, 1996; Gibert et al., 1998; Fleet and Knipe, 2000; Stefánsson and Seward, 2003, 2004; Dadze and Kashirtseva, 2004; Tagirov et al., 2005, 2006). In the cited works the composition and stability of chloride and hydrosulfide complexes was determined via the measurements of Au solubility as a function of pH, $f(H_2)$, and sulfur activity at reduced *Red*/*Ox* conditions, where S^{2-} oxidation state of sulfur predominates, and H_2S/HS^- are the dominant sulfur species. Natural ore-forming systems, however, can transport ore metals in wide range of *Red*/*Ox* conditions from reduced to oxidized. For example, hydrothermal systems associated with volcanogenic massive sulfide (VMS) deposits and their modern analogues – submarine hydrothermal systems, are characterized mostly by reduced conditions (Large et al., 1977; Kawasumi and Chiba, 2017). In these systems deposition of ore sulfides, which are often enriched in Au, takes place in response to the drop of temperature, pH, $f(O_2)$, and $\sum S$. In contrast to VMS deposits, most of the porphyry Cu-(Mo)-(Au) deposits are associated with oxidized magmas ($\log f(O_2) > FMQ + 2$, where FMQ is fayalite-magnetite-quartz oxygen buffer, c.f. Sun et al., 2015). In these magmas SO_4^{2-} predominates over reduced sulfur species. The hydrothermal fluids inherited high oxidation potential from the oxidized volatile species such as SO_2 and SO_3 that were degassed from the parental magma. Formation of the stable Au complexes with oxidized S species in addition to Au-HS complexes can increase the fluid transport capacity with respect to Au. In addition, sulfide-rich hydrothermal fluids often contain significant concentrations of chlorides that can increase the concentration of dissolved Au via the formation of the mixed hydrosulfide-chloride Au-HS-Cl species. In contrast to chloride complexes $AuCl°_{(aq)}$ and $AuCl_2^-$, which are responsible for Au transport in acidic fluids, mixed HS-Cl species can form at weakly-acidic and near-neutral pH, where $Au(HS)_2^-$ is the dominant Au complex in the absence of chlorides. Therefore, more experimental data are needed to characterize the chemical state

(composition of aqueous complexes and their stability) of Au in oxidized sulfide environments, including chloride-rich fluids.

In accord with the available thermodynamic data (e.g., SUPCRT92 database, Johnson et al., 1992), the dominant S species in acidic high temperature (>300 °C) oxidized hydrothermal sulfide-rich fluids are H_2S (S^{-2} oxidation state), SO_2 (or its hydrated form – sulfurous acid H_2SO_3, S^{+4} oxidation state), with minor contribution of the completely dissociated H_2SO_4 (S^{+6} oxidation state) in the form of HSO_4^-. At near-neutral and alkaline pH the role of S^{+4} decreases and the dominant S species are H_2S/HS^- and HSO_4^-/SO_4^{2-} with subordinate amount of SO_3^{2-}/HSO_3^-, which also can form complexes like $Au(SO_3)_2^{3-}$ (the latter complexes are known to be stable in alkaline solutions at ambient temperature, Peshevitsky et al., 1976). In addition, radical species (S_3^-) exist in solutions where log $f(O_2)$ is controlled by sulfide-sulfate buffer (Giggenbach, 1974; Pokrovski and Dubessy, 2015). Formation of stable Au complexes with S_3^- was suggested by Mei et al. (2014) on the basis of *ab initio* molecular dynamics simulations. The $Au(HS)S_3^-$ complex was found to be important for the hydrothermal Au transport by means of analysis of the solubility of Au and X-ray absorption spectroscopy studies of the oxidized sulfide system (Pokrovski et al., 2015).

In the current study, we used synchrotron X-ray absorption spectroscopy (XAS) to compare the speciation of Au in sulfide-rich hydrothermal fluids at contrasting *Red*/*Ox* conditions. We recorded Au L_3-edge X-ray absorption spectra for the systems of 3 types: i) reduced, where the speciation of S is dominated by H_2S/HS^-, ii) oxidized with H_2S/SO_4^{2-} as the dominant species, and iii) oxidized chloride-rich with NaCl added to the oxidized sulfide system. The X-ray absorption near edge structure/extended X-ray absorption fine structure (XANES/EXAFS) spectra measurements were performed in high energy resolution fluorescence detection (HERFD) mode (Glatzel and Bergman, 2005) which allows observation of important spectral features not manifested in total fluorescence yield (TFY) geometries (Tagirov et al., 2016; Trigub et al., 2017). The composition of Au complexes was derived by the fitting of conventional EXAFS spectra with the aid of IFEFFIT software package (Ravel and Newville, 2005), and by EXAFS spectra fitting performed

with the aid of Reverse Monte-Carlo method (Timoshenko et al., 2012). Additional information on the effect of the system composition on the stoichiometry of Au complexes was provided by simulation of the EXAFS and XANES spectra using the atomic/molecular structures generated by means of *ab initio* molecular dynamics (Gianozzi et al., 2009). Interpretation of the XAS spectra together with the measurements of Au solubility performed at 450 °C/1000 bar in oxidized sulfide system, show that the chemical states of Au in high-temperature reduced and oxidized sulfide (±Cl) systems are identical and corresponds to $Au(HS)_2^-$/AuHS° complexes. The calculated Au solubility constants are in close agreement with values reported previously.

2. Methods

In this section experimental methods used for the measurements of the solubility of Au and X-ray absorption spectroscopy measurements are described. Details on the computational methods, including thermodynamic calculations, EXAFS spectra fitting, *ab-initio* molecular dynamics simulations, and calculations of theoretical XANES/EXAFS spectra are provided in supplemental information.

2.1. Gold solubility determinations

Hydrothermal Au solubility experiments were carried out at 450 °C and 1000 bar pressure using Ti autoclaves (VT-8 alloy) with an internal volume of ~25 ml. A strip of Au foil was attached to the Ti partition in the upper part of the autoclave. The autoclaves were loaded with the necessary amount of $S_{(cr)}$, distilled water degassed by boiling and saturated with Ar, or solution of NaOH. The stock ~ 2*m* NaOH solution was prepared from the concentrated ultra pure base and standardized against HCl solution, which concentration was determined against tris(hydroxymethyl)-aminomethane (Trizma-base, Aldrich) with methyl red as an indicator. Pressure in the autoclaves was controlled by the degree of filling in accord with *PVT* data for NaCl-H_2O system. The closed autoclaves were placed into the gradientless furnaces preheated to 450 °C. At the end of the three

weeks period the autoclaves were quenched in cold water. The concentration of Au in quench solutions and in solutions obtained by flushing of the autoclave walls with hot aqua regia was determined by means of ICP-MS. The method of samples preparation is described in detail in Tagirov et al. (2013). For the ICP-MS analyses samples were diluted with 2M HCl to fall within the necessary concentration range (< 100 ppb) and eliminate effect of NaCl, which was formed due to interaction of alkaline solutions with aqua regia.

2.2. XAS spectroscopic measurements

The experimental setup used for spectroscopic experiments was described in detail in Tagirov et al. (2016) and Trigub et al. (2017) and, therefore, will be only briefly outlined here. XAS spectra were collected at high-brilliance X-ray absorption and X-ray emission spectroscopy undulator beamline ID26 of the European Synchrotron Radiation Facility (ESRF) at Grenoble. The flux of the incident X-ray beam was approximately $2 \cdot 10^{13}$ photon s^{-1} on the sample position. XANES spectra were measured in the high energy resolution fluorescence detection (HERFD) mode using an X-ray emission spectrometer (Glatzel and Bergmann, 2005; Kvashnina and Scheinost, 2016). The sample, analyzer crystal, and photon detector (silicon drift diode) were arranged in a vertical Rowland geometry. The Au XANES/EXAFS HERFD spectra at the L_3-edge were obtained by recording the intensity of the Au $L\alpha_1$ emission line (9713 eV) as a function of the incident energy. The intensity was normalized to the incident flux.

In the heating experiment a small piece of Au wire (1.5 mm long) was loaded into a silica glass capillary (Polymicro Technologies™, 600 μm OD, 400 μm ID, 20 mm length) filled with solution of $Na_2S_2O_3$ or NaOH. In the experiment with reduced system a weighted amount of $Al_2S_{3(cr)}$ was loaded into the capillary filled with NaOH solution. The Al_2S_3 was synthesized by heating stoichiometric quantities of ultra pure Al and S in the evacuated silica glass ampoule. Heated $Al_2S_{3(cr)}$ reacted with water and produced H_2S,

$$Al_2S_{3(cr)} + 4\ H_2O = 2\ AlOOH_{(cr)} + 3\ H_2S \quad . \quad (1)$$

In the *in situ* XAS measurements hermetically sealed capillaries were placed into a microtomography furnace (Bellet et al., 2003). Temperature readings were calibrated at an accuracy of ±5 °C with a *K*-type thermocouple placed instead of the capillary.

3. Results and discussion

3.1. Gold solubility

Results of the Au solubility experiments are collected in Table 1. Assuming that at the experimental parameters the dominant sulfur species are H_2S/HS^-, SO_4^{2-}, HSO_3^-/SO_3^{3-}, $H_2S_2O_3^{2-}$, and S_3^-, and bearing in mind that the Au-SO_4^{2-} complexes are weak (Peshevitsky et al., 1976), formation of the sulfur-bearing Au complexes can be described by the following reactions,

$$Au_{(cr)} + 2\ H_2S°_{(aq)} = Au(HS)_2^- + H^+ + 0.5\ H_{2(g)} \qquad K_{(Au(HS)_2^-)} \qquad (2)$$

$$Au_{(cr)} + 4\ H_2S°_{(aq)} = Au(HS)S_3^- + H^+ + 3\ H_{2(g)} \qquad K_{(Au(HS)S_3^-)} \qquad (3)$$

$$Au_{(cr)} + 6\ H_2S°_{(aq)} = Au(S_3)_2^- + H^+ + 5.5\ H_{2(g)} \qquad K_{(Au(S_3)_2^-)} \qquad (4)$$

$$Au_{(cr)} + 2\ H_2S°_{(aq)} + 6\ H_2O_{(l)} = Au(HSO_3)_2^- + 6.5\ H_{2(g)} \qquad K_{(Au(HSO_3)_2^-)} \qquad (5)$$

$$Au_{(cr)} + 2\ H_2S°_{(aq)} + 6\ H_2O_{(l)} = Au(SO_3)_2^{3-} + 3\ H^+ + 6.5\ H_{2(g)} \qquad K_{(Au(SO_3)_2 3-)} \qquad (6)$$

$$Au_{(cr)} + H_2S°_{(aq)} = AuHS°_{(aq)} + 0.5\ H_{2(g)} \qquad K_{(AuHS)} \qquad (7)$$

$$Au_{(cr)} + 2\ H_2S°_{(aq)} = HAu(HS)_2° + 0.5\ H_{2(g)} \qquad K_{(HAu(HS)_2)} \quad . \qquad (8)$$

The Au-$S_2O_3^{2-}$ complexation is not considered here because, as will be shown in the next section, XANES spectra analysis ruled out formation of these species at the experimental parameters. The experimental data on the solubility of Au were used for the calculation of Gibbs energies of the aqueous Au complexes and corresponding solubility reaction constants. Results of the calculations are presented in Table 2. Figure 1 displays the difference between the calculated and the experimental values of the Au solubility. The $Au(HS)_2^-$/AuHS° model matches the experimental data better than other models of Au speciation. Thus, in accord with our data, gold in oxidized sulfide

system dissolves with the formation of AuHS° (acidic pH) and $Au(HS)_2^-$ (weakly acidic to alkaline pH) complexes.

This speciation model can be checked via analysis of the Au solubility as a function of pH and sulfur concentration. The concentration of Au directly correlated with pH in near-neutral to weakly-acidic solutions (Fig. 2a). The slope of the solubility curve vs. pH is close to +1 which implies that the $Au(HS)_2^-$ predominates (Eq. 2). At acidic pH ~ 3 the concentration of dissolved Au increases with increase of the H_2S concentration. The slope +1.2 (Fig. 2b) indicates that the dominant complex is $AuHS°_{(aq)}$ (Eq. 7) with minor contribution of other species with higher number of ligands - $Au(HS)_2^-$. The formation of $HAu(HS)_2°$ can be ruled out as the concentration of this complex is pH-independent, but increases as the 2nd power of H_2S molality (Eq. 8, slope log *m*(Au) vs. log *m*(H_2S) is +2).

The $Au(HS)_2^-/AuHS°_{(aq)}$ solubility constants, calculated from the experimental data on Au solubility, were compared with the literature values (Table 2). Our results for $Au(HS)_2^-$ are in excellent agreement with the data of Fleet and Knippe (2000), who have measured the Au solubility at 100 – 400 °C, 1500 bar in reduced sulfide system containing 20.6 *m* H_2S. At this extremely high H_2S concentration the *Red-Ox* potential of the system is controlled by $H_2S/S°$ couple. The value of $K_{(Au(HS)_2^-)}$ predicted by Sverjensky et al. (1997) with the aid of the HKF (Helgeson-Kirkham-Flowers) equation of state and model correlations are based on the experimental Au solubility data reported in Shenberger and Barnes (1989) for 250 °C and saturated vapor pressure. The value of Sverjensky et al. (1997) is also in excellent agreement with our data. Baranova and Zotov (1998) and Dadze and Kashirtseva (2004) measured the solubility of Au in reduced media at temperatures up to 350 °C (these data are not shown in Table 2 because of lower experimental temperatures). In these experiments H_2S was produced by thioacetic acid hydrolysis. The measured values of the solubility of Au were much higher than those determined by other researchers. For example, at 300 °C and 300-500 bar pressure log $K_{Au(HS)_2^-}$ falls within -0.3 ÷ -0.6 range. Extrapolation of these data to 450 °C results in positive values of log $K_{Au(HS)_2^-}$ which are at least one log unit higher than the value of

log $K_{Au(HS)_2^-}$ = -0.9 determined in the present study. Stefánsson and Seward (2004) measured the solubility of Au in the diluted H_2S/NaOH/HCl solutions with control of dissolved hydrogen concentration, and calculated $AuHS°_{(aq)}$ and $Au(HS)_2^-$ formation constants for 100 – 500 °C temperature range. The difference between the data of Stefánsson and Seward (2004) with results of the present study is 0.75 log units and, as will be discussed below, can be attributed to the uncertainties in calculation of the sulfur speciation of the oxidized sulfide fluids studied in the present work. Data of Tagirov et al. (2005) were obtained in a chemical system which included silicate and sulfide mineral assemblages that controlled pH and sulfur activity, respectively. The calculated $Au(HS)_2^-$ formation constants are in close agreement with the values reported by Stefánsson and Seward (2004). The values of solubility of Au determined by Gibert et al. (1998) in weakly acidic fluids in the system with mineral buffers also are in good agreement with data reported in Stefánsson and Seward (2004) (see Fig. 12 in Stefánsson and Seward, 2004).

To summarize the discussion about the Au solubility, we note that all the above studies and the present work, are consistent with the predominance of $Au(HS)_2^-/AuHS°_{(aq)}$ complexes in both reduced and oxidized sulfide systems. All the published so far values and our experimental $K_{Au(HS)_2^-}$ value fall within 1 log unit interval (-0.9 ÷ -1.9, neglecting pressure variations) independently of the *Red/Ox* conditions in the experimental system. These discrepancies in $K_{Au(HS)_2^-}$ can result from insufficiently accurate chemical and thermodynamic description of complex systems where sulfur presents in several oxidation states. In particular, for oxidized sulfide system the calculated pH and $f(O_2)$ are highly uncertain because thermodynamic values and dissociation constants for sulfur-bearing acids and their salts (e.g., NaHS, Na_2SO_3, $NaHSO_3$, Na_2SO_4, NaS_3 etc.) are not well characterized. The most accurate values of $K_{Au(HS)_2^-}$ were obtained from the experiments performed in the simple system where sulfur presents in S^{2-} oxidation state (Stefánsson and Seward, 2004). At the same time, at low temperatures, where in oxidized system the concentration of polysulfide ions (S_nS^{2-}, t < 150 °C) and radicals (e.g., S_3^-, 150 °C < t < 300 °C) becomes significant (Giggenbach, 1974), formation of Au complexes with these ligands can enhance Au mobility (c.f.

Berndt et al., 1994). At acidic values of pH, gold dissolves with the formation of $AuHS°_{(aq)}$. The calculated $K_{(AuHS)}$ value (Eq. 7) is in good agreement with the literature data (Table 2).

3.2. XANES spectra analysis

Gold L_3-edge HERFD-XANES spectra of the experimental solutions and reference compounds are shown in Fig. 3, positions of the main features of the spectra are listed in Table 3. Fig. 3 shows that the spectra of all experimental solutions are identical. Positions and intensities of two main spectral features for reduced (H_2S/NaOH) and oxidized ($Na_2S_2O_3$ and $Na_2S_2O_3$/NaCl) sulfide systems are close to each other. The difference between the positions of the first two features ($\Delta_{B\text{-}WL}$ in Table 3) is the same for all the spectra: it is clearly illustrated in the insert of Fig. 3 where the spectra of the oxidized and reduced systems are compared. The only difference between the spectra is ~0.5 eV shift of the white line position in the spectra of 3.6*m* $Na_2S_2O_3$ solution (Table 3). The observed shift can result from the high concentration of charged species in the experimental solution, and disappears in less concentrated 1.1*m* $Na_2S_2O_3$ fluid at higher temperature (experiment cap1). These data provide significant evidence that the local structural environment of Au in sulfide-rich fluids is independent of the system composition, *Red/Ox* state, and the experimental *PT*-parameters. This suggestion was checked with the aid of *ab initio* molecular dynamics simulations reported in the following sections. Note also that the $\Delta_{B\text{-}WL}$ values of experimental solutions are different from those of the reference systems - $Au(S_2O_3)_2^{3-}$ complex and $Au_2S_{(cr)}$ (6.5 vs. 8.2 vs. 8.9 eV, respectively). Despite the fact that the Au-S distance in the reference systems are close to the Au-S distance in aqueous Au (hydro)sulfide complexes, the S and Au (for crystalline phase) atoms present in the distant coordination shells of Au in $Au(S_2O_3)_2^{3-}$ and $Au_2S_{(cr)}$ which can result in the observed difference between the spectra.

3.3. Au aqueous complex composition from EXAFS spectra fitting (ARTEMIS code)

In the previous studies (Pokrovski et al., 2009; Mei et al., 2013) it was shown that the distance between Au and the nearest S atom calculated using quantum chemistry and *ab initio* molecular dynamics is independent of the composition of aqueous complex and falls within 2.30 ± 0.01Å for $Au(HS)_2^-$, $AuHS(SO)_2°$, $Au(HSO_3)_2^-$, $Au(SO_3)_2^{3-}$, $Au(HS)S_3^-$, and $Au(S_3)_2^-$. Therefore, the position and intensity of the first maximum of the Fourier transform (FT) of EXAFS function is insensitive to the presence of an anion (S^{2-} or O^{2-}) in the distant coordination shell. In order to determine the *k*- and *R*- ranges for which EXAFS is sensitive to the composition of the distant coordination shells, the shape of the FT was examined as a function of *k*-range (Fig. 4). The calculated FT functions demonstrate that at $R > 3$ Å, where the atoms located in the distant coordination shells can contribute to EXAFS, the FT fine structure becomes clearly visible only for $k \geq 11$ $Å^{-1}$. The structure of EXAFS FT obtained for oxidized sulfide systems (cap8 and cap21, bottom of Fig. 4) comprises three peaks with different positions and intensities located at $3 < R < 4.5$ Å. Despite the fact that both systems are oxidized, the structures of the FTs seem to be different. The best quality EXAFS spectrum was collected for experiment cap21. Therefore, this spectrum was used to examine the possibility of the formation of complexes with- and without an anion in the second coordination shell. Table 4 and Fig. A1 report the results of EXAFS spectra fitting performed with the aid of ARTEMIS computer code (which is a part of IFEFFIT software package). As an example of Au complex with an anion in the second coordination shell we used $Au(HS)S_3^-$ which was suggested as the dominant Au complex in oxidized high-temperature sulfide solutions by Pokrovski et al. (2015). Results of the fitting procedures (Table 4) are consistent with the presence of 2 S atoms located in the first coordination shell of Au at 2.29±0.02 Å for both $Au(HS)_2^-$ and $Au(HS)S_3^-$ complexes. Our data demonstrate that both models based on $Au(HS)_2^-$ and $Au(HS)S_3^-$ species fit the fine EXAFS FT structure at $R > 3$ Å with nearly equal accuracy. This can be explained by the high value of Debye-Waller factor $\sigma^2 = 0.025$ for Au-S_2 bond, which makes the spectrum weakly sensitive to the presence of the S atom (labeled here as S_2) in the second coordination shell. Note that the theoretical fits do not reproduce the third peak of the FT with

maximum at ~4.3 Å. Therefore, in addition to ARTEMIS computer code, other method of EXAFS spectra fitting (Reverse Monte-Carlo, RMC), and comparison of the experimental spectra with results of *ab initio* molecular dynamics (AIMD) were applied to obtain parameters of the distant coordination shells of Au complexes.

3.4. AIMD simulations

Ab initio molecular dynamics simulations were performed to obtain atomic configurations for subsequent modeling of EXAFS and XANES spectra. Geometries of aqueous Au complexes generated via the AIMD simulations are listed in Table 5, thermochemical properties of simulation boxes are listed in Table 6. Data collected in Table 6 imply that stabilities of all the modeled Au-S-HS complexes are equivalent within the calculation uncertainty. The calculated radial distribution functions $g_{ij}(r)$ and coordination numbers of Au are presented in Fig. A2, A3, and A4. The radial distribution function of Au-S (complexes $Au(HS)S_3^-$ and $Au(S_3)_2^-$, Fig. A3) has a weak diffuse peak located between 3 and 4 Å. This implies that the S_2 atom position is not well defined (S_2 stands for the sulfur atom in the second coordination shell of Au), and the Au-S_2 distance as well as the Au-S_1-S_2 angle fluctuates widely. Consequently, the absence of the "rigid" geometry results in high value of the Debye-Waller parameter for S_2 atom (Table 4) and makes difficult (if at all possible) determination of the local atomic structure parameters of complexes with an anion in the second coordination shell. Another interesting peculiarity revealed by the AIMD simulations is that the coordination of Au by Na is the highest for $Au(HS)S_3^-$ model (Fig A3). In this system the Au-Na radial distribution function has two maxima between 3.5 and 5 Å. The coordination number (*CN*) of Na is 1 at ~4 Å and reaches 3.5 at a distance of 6 Å, whereas the CN_{Na} is only 1.5 and 1 at 6 Å distance for $Au(HS)_2^-$ and $Au(S_3)_2^-$, respectively.

3.5. Results of EXAFS spectra simulations (AIMD and RMC methods)

Results of EXAFS spectra modeling by means of the RMC and AIMD methods are shown in Fig. 5a,b. Parameters of the local atomic environment of Au complexes obtained by RMC fits are listed in Table A3. Comparison of the experimental and theoretical spectra lead to conclusion that RMC fitting always is in better agreement with the experimental spectra than theoretical spectra based on the AIMD atomic configurations. The reason behind it is that the RMC-EXAFS analysis is aimed to minimize the difference between the experimental and calculated signals, whereas the AIMD-EXAFS spectra are calculated from the fixed atomic configurations.

In case of Au-HS-Cl system (cap8, Fig. 5a) the best agreement between the experimental and calculated spectra is observed for $Au(HS)_2^-$ complex. This is true for both RMC-EXAFS and AIMD-EXAFS simulations, although the agreement is better for RMC-EXAFS for the reasons indicated above. In the case when chloride ion is included into the first coordination shell of Au with the formation of mixed $Au(HS)Cl^-$ complex, the AIMD simulation underestimates the amplitude of the EXAFS function oscillations as well as the intensity of the first FT peak. Therefore, the formation of mixed Au-HS-Cl complex can be ruled out. The oscillations of EXAFS signal in the region of multiple-scattering contributions at $R > 3$ Å are poorly reproduced by AIMD-EXAFS. Despite the fact that the FT of both experimental and AIMD-EXAFS signals in this region consists from two main peaks, their intensity in the theoretical spectra is underestimated, and their maxima are located at lower values of R compared to the experimental spectra.

For experiment cap21 (oxidized system, 3.6*m* $Na_2S_2O_3$ loaded into the capillary) three models were tested: $Au(HS)_2^-$, $Au(HS)S_3^-$, and $Au(S_3)_2^-$ (Fig. 5b). The best agreement between the theoretical and experimental spectra was observed for the RMC-EXAFS fit based on the $Au(S_3)_2^-$ model (right-side panel of Fig. 5b). In this simulation the theoretical spectra reproduces both intensity/position of the first peak in the FT corresponding to the S_1 ligands contributions, as well as the structure of the FT at $R > 3$ Å which consists of three distinct features with the most intense one located at ~3.7 Å. The AIMD-EXAFS simulation is almost equivalent for all three models, with slightly better agreement with the experimental spectra for $Au(HS)S_3^-$. Nonetheless, the structure of

the distant FT region, where contributions from both multiple-scattering and Au-S_2-Au single-scattering paths are located, is poorly reproduced by the theoretical calculations for all three complexes. One can conclude that the interpretation of EXAFS spectra based on the AIMD method cannot result in unambiguous determination of the composition of Au-HS-S complex because of superposition of multiple-scattering contributions with small effect of sulfur atoms located in the distant coordination shells.

3.6. Theoretical XANES spectra

Simulations of HERFD-XANES spectra by means of AIMD approach are presented in Fig. 6. Simulation performed for experiment cap33 (Fig. 6a) was based on the $Au(HS)_2^-$ model. In the reduced sulfide system, where H_2S/HS^- are the dominant sulfur species, the formation of Au complexes with oxidized sulfur species, including S radicals and S^{+4} anions can be neglected. This simulation resulted in the spectrum with the WL intensity underestimated in comparison with the experimental HERFD-XANES one. The AIMD-XANES simulations performed for experiment cap21 (oxidized system, H_2S/SO_4^- dominate sulfur speciation) resulted in three different spectra. Figures 6b,c,d show that the shape of the calculated spectra is strongly dependent on the complex composition. For $Au(HS)_2^-$ model the WL intensity is much lower than the intensity of the second feature, for $Au(HS)S_3^-$ the first and the second features intensities are almost equal, whereas for $Au(S_3)_2^-$ WL is the most intense HERFD-XANES feature. Calculations of Lowdin and Bader partial atomic charges showed that the observed differences stem from the atomic charges redistribution (Table A4). Replacement of HS^- with S_3^- results in increase of the unoccupied 5*d* DOS of Au (and, consequently, of the positive charge on Au), which yields the increase of the WL intensity predicted for Au complexes with S_3^- radical. As the experimental spectra for reduced and oxidized systems (cap33 and cap21, respectively) are identical, whereas the shape of the spectrum is predicted to be highly sensitive to the composition of the Au complex, we conclude that the same Au complex - $Au(HS)_2^-$ - predominates in both systems. Formation of other complexes with oxidized sulfide

species is also possible, but the concentrations of these complexes are not high enough to be detected by means of the HERFD-XAS.

4. Concluding remarks

The Au speciation in aqueous fluids of different *Red*/*Ox* states and chemical compositions has been explored by the combination of HERFD-XAS measurements of Au dissolved in aqueous fluids with *ab initio* molecular dynamics simulations, and measurements of Au solubility in oxidized sulfide fluid. The solubility of Au in oxidized sulfide-bearing fluids (sulfide/sulfate equilibrium controls the *Red*/*Ox* state) decreases linearly with decreasing pH from alkaline to weakly-acidic at supercritical *PT*-parameters (450 °C, 1000 bar). The experimental Au solubility data matches best the model of $Au(HS)_2^-$ and $AuHS°_{(aq)}$ complexes. Stability constants for these Au complexes are in reasonable agreement with published literature values. Interpretation of EXAFS spectra recorded at Au L_3-edge reveals that, independently of the *Red*/*Ox* state (sulfide or sulfide/sulfate systems) and *PT* – conditions (350 – 450 °C, 500 bar) two S atoms forms the first coordination shell of Au at 2.29±0.02 Å. The same local atomic environment of Au was monitored in H_2S/SO_4^{2-}/NaCl fluid which rules out the formation of mixed Au-HS-Cl species. It is shown that the interpretation of EXAFS spectra solely is not sufficient to make a conclusion about the presence of a specific anion in a distant coordination shell of Au and, thereby about the formation of Au complexes with SO_3^{2-}, HSO_3^-, or sulfur radical species S_3^-. To discriminate between the speciation of Au in reduced and oxidized sulfide systems we recorded Au L_3-edge HERFD-XANES spectra in reduced H_2S – bearing fluid, and in oxidized one where H_2S/SO_4^{2-} equilibrium controlled the *Red*/*Ox* state. The recorded spectra were identical which argues for similar character of Au speciation in fluids of contrasting *Red*/*Ox* states. Results of *ab initio* molecular dynamics simulations confirm this conclusion. It is shown that formation of complexes with S atoms in the distant coordination shells (Au-HS-S_3^- or Au-S_3^-) would result in prominent changes of the HERFD-XANES. This means that Au-HS complexes ($Au(HS)_2^-$ and $AuHS°_{(aq)}$) predominate in sulfide-rich supercritical fluids

independently of their oxidation state, and the decrease of pH and temperature causes Au deposition with the formation of Au-bearing ores.

Nonetheless, the formation of stable Au complexes with S^{4+} species (sulfite and hydrosulfite ion), $S_2O_3^{2-}$ (thiosulfate), S_3^- (sulfur radical), S_nS^{2-} (polysulfide) and HS_nS^- (hydropolysulfide) ions is possible (Peshevitsky at al., 1976; Giggenbach, 1974; Mei et al., 2013) and can affect the speciation of Au in oxidized systems at low temperatures (<300 °C), where these ligands are available in sufficient concentrations. In these "oxidized" solutions (or, more precisely, solutions of intermediate oxidation degree where sulfur can adopt various oxidation states including intermediate ones), the above mentioned complexes of Au can compensate the effect of decreasing pH and temperature and stabilize dissolved Au. Formation of Au-S_3^- complexes at high *PT*-conditions also cannot be ruled out and may enhance the mobility of Au in high-pressure oxidized sulfide fluids due to increase of the S^{3-} stability and concentration (Pokrovski and Dubessy, 2015). More experimental data pertinent to fluids produced in subduction zones are necessary in order to elucidate the speciation of Au at high *PT*-conditions.

Acknowledgements

The authors acknowledge the ESRF for the beamtime allocation under proposal ES-360. The help and support of Pieter Glatzel during the beam time is greatly appreciated. We thank Hugo Vitoux for outstanding technical support during the *in-situ* experiment with micro-furnace at ID26 beamline. The authors are grateful to Nina N. Baranova for her help during the experimental work and to Alexander V. Zotov for the help in planning the experiments and useful discussions during the manuscript preparation. Pavel V. Selivanov is acknowledged for the assistance in preparation of the synchrotron experiments, and Dmitry A. Chareev - for the synthesis of Al_2S_3. The results of this work were obtained using the computational resources of MCC NRC "Kurchatov Institute" (http://computing.kiae.ru/). Chemical analyses were carried out at the "IGEM-Analytica" laboratory. This study was supported by the Russian Science Foundation grant No. 17-17-01220.

References

Baranova, N.N, Zotov, A.V., 1998. Stability of gold sulphide species ($AuHS°_{(aq)}$ and $Au(HS)_2^-$) at 300, 350°C and 500 bar. Min. Magazine 62A, 116-117.

Bellet, D., Gorges, B., Dallery, A., Bernard, P., Pereiro, E., Baruchel, J., 2003. A 1300 K furnace for in situ X-ray microtomography. J. Appl. Cryst. 36, 366-367.

Benning, L.G, Seward, T.M., 1996. Hydrosulphide complexing of Au (I) in hydrothermal solutions from 150–400°C and 500–1500 bar**.** Geochim. Cosmochim. Acta 60, 1849-1871.

Berndt, M.E., Buttram, T., Earley III, D., Seyfried Jr, W.E., 1994. The stability of gold polysulfide complexes in aqueous sulfide solutions: 100 to 150°C and 100 bars. Geochim. Cosmochim. Acta 58, 587-594.

Dadze, T.P., Kashirtseva, G.A., 2004. Experimental study of gold solubility in sulfide-bearing hydrothermal solutions, in: Zharikov, V.A., Fedkin, V.V. (Eds.), Experimental mineralogy. Science, Moscow, pp. 315-326 (in Russian).

Fleet, M.E., Knipe, S.W., 2000. Solubility of native gold in H-O-S fluids at 100-400 °C and high H_2S content. J. Solut. Chem. 29, 1143-1157.

Giannozzi, P., Baroni, S., Bonini, N., Calandra, M., Car, R., Cavazzoni, C., Ceresoli, D., Chiarotti, G.L., Cococcioni, M., Dabo, I., and others, 2009. QUANTUM ESPRESSO: a modular and open-source software project for quantum simulations of materials. J. Phys. Cond. Matt. 21, 395502.

Gibert, F., Pascal, M.-L., Pichavant, M., 1998. Gold solubility and speciation in hydrothermal solutions: experimental study of the stability of hydrosulphide complex of gold (AuHS°) at 350 to 450°C and 500 bars. Geochim. Cosmochim. Acta 62, 2931-2947.

Giggenbach, W.F., 1974. Equilibria involving polysulfide ions in aqueous sulfide solutions up to 240 °C. Inorg. Chem. 13, 1724-1730.

Glatzel, P., Bergman, U., 2005. High resolution 1s core hole X-ray spectroscopy in 3d transition metal complexes - electronic and structural information. Coord. Chem. Rev. 249, 65-95.

Johnson, J.W., Oelkers, E.H., Helgeson, H.C., 1992. SUPCRT92: A software package for calculating the standard molal thermodynamic properties of minerals, gases, aqueous species, and reactions from 1 to 5000 bar and 0 to 1000°C. Comp. Geosci. 18, 899-947.

Kawasumi, S., Chiba, H., 2017. Redox state of seafloor hydrothermal fluids and its effect on sulfide mineralization. Chem. Geol. 451, 25-37.

Kvashnina, K.O., Scheinost, A.C., 2016. A Johann-type X-ray emission spectrometer at the Rossendirf Beamline. J. Synch. Radiation 23, 836–841.

Large, R.R., 1977. Chemical evolution and zonation of massive sulfide deposits in volcanic terrain. Econ. Geol. 72, 549-572.

Mei, Y., Sherman, D.M., Liu, W., Brugger, J., 2013. Complexation of gold in S_3^--rich hydrothermal fluids: Evidence from ab-initio molecular dynamics simulations. Chem. Geol. 347, 34-42.

Peshevitsky, B.I., Belevantsev, V.I., Zemskov, S.V., 1976. New data on chemistry of gold compounds in solutions. Izvestiya Sibirskogo Otdeleniya AN SSSR, ser. Khimicheskih nauk, No. 4, vip. 2, pp. 24-45 (in Russian).

Pokrovski, G.S., Dubessy, J., 2015. Stability and abundance of the trisulfur radical ion S_3^- in hydrothermal fluids. Earth Plan. Sci. Let., 411, 298-309.

Pokrovski, G.S., Kokh, M.A., Guillaume, D., Borisova, A.Y., Gisquet, P., Hazemann, J.-L., Lahera, E., Del Net, W., Proux, O., Testemale, D., Haigis, V., Jonchière, R., Ari, P., Seitsonen, A.P., Ferlat, G., Vuilleumier, R., Saitta, A.M., Boiron, M.-C., Dubessy, J., 2015. Sulfur radical species form gold deposits on Earth. PNAS 112, 13484–13489.

Pokrovski, G.S., Tagirov, B.R., Schott, J., Hazemann, J.-L., Proux, O., 2009. A new view on gold speciation in sulfur-bearing hydrothermal fluids from in situ X-ray absorption spectroscopy and quantum-chemical modeling. Geochim Cosmochim Acta 73, 5406-5427.

Seward, T.M., 1973. Thio complexes of gold and the transport of gold in hydrothermal ore solutions. Geochim. Cosmochim. Acta 37, 379–399.

Shenberger, D.M., Barnes, H.L., 1989. Solubility of gold in aqueous sulfide solutions from 150 to 350 °C. Geochim. Cosmochim. Acta 53, 269-278.

Stefánsson, A., Seward, T.M., 2003. Stability of chloridogold(I) complexes in aqueous solutions from 300 to 600°C and from 500 to 1800 bar. Geochim. Cosmochim. Acta 67, 4559-4576.

Stefánsson, A., Seward, T.M., 2004. Gold(I) complexing in aqueous sulphide solutions to 500°C at 500 bar. Geochim. Cosmochim. Acta 68, 4121-4143.

Sun, W., Huang, R.-F., Li, H., Hu, Y.-B., Zhang, C.-C., Sun, S.-J., Zhang, L.-P., Ding, X., Li, C.-Y., Zartman, R.E., Ling, M.-X., 2015. Porphyry deposits and oxidized magmas. Ore Geol. Rev. 65, 97-131.

Sverjensky, D.A., Shock, E.L., Helgeson, H.C., 1997. Prediction of the thermodynamic properties of aqueous metal complexes to 1000°C and 5 kb. Geochim. Cosmochim. Acta 61, 1359-1412.

Tagirov, B.R., Salvi, S., Schott, J., Baranova, N.N., 2005. Experimental study of gold-hydrosulphide complexing in aqueous solutions at 350–500°C, 500 and 1000 bars using mineral buffers. Geochim. Cosmochim. Acta 69, 2119-2132.

Tagirov, B.R., Baranova, N.N., Zotov, A.V., Schott, J., Bannykh, L.N., 2006. Experimental determination of the stabilities of $Au_2S_{(cr)}$ at 25 °C and $Au(HS)_2^-$ at 25–250 °C. Geochim. Cosmochim. Acta 70, 3689-3701.

Tagirov, B.R., Baranova, N.N., Zotov, A.V., Akinfiev, N.N., Polotnyanko, N.A., Shikina, N.D., Koroleva, L.A., Shvarov, Yu.V., Bastrakov, E.N., 2013. The speciation and transport of palladium in hydrothermal fluids: Experimental modeling and thermodynamic constraints. Geochim. Cosmochim. Acta 117, 348-373.

Tagirov, B.R., Trigub, A.L., Kvashnina, K.O., Shiryaev, A.A., Chareev, D.A., Nickolsky, M.S., Abramova, V.D., Kovalchuk, E.V., 2016. Covellite CuS as a matrix for “invisible” gold: X-ray spectroscopic study of the chemical state of Cu and Au in synthetic minerals. Geochim. Cosmochim. Acta, 191, 58–69.

Trigub, A.L., Tagirov, B.R., Kvashnina, K.O., Chareev, D.A., Nickolsky, M.S., Shiryaev, A.A., Baranova, N.N., Kovalchuk, E.V., Mokhov, A.V., 2017. X-ray spectroscopy study of the chemical state of “invisible” Au in synthetic minerals in the Fe-As-S system. Am. Mineral. 102, 1057-1065.

Zotov, A.V., Baranova, N.N., Dar’yina, T.G., Bannykh, L.M., 1991. The solubility of gold in aqueous chloride fluids at 350–500°C and 500–1500 atm: Thermodynamic parameters of $AuCl_2^-{}_{(aq)}$ up to 750°C and 5000 atm. Geochem. Intern. 28, 63–71.

Figure captions

Fig. 1. Deviation of calculated from experimental concentrations of Au as a function of calculated pH. Gold speciation models used for thermodynamic calculations are indicated at the top of each figure.

Fig. 2. Gold solubility as a function of calculated pH (a) and $H_2S°_{(aq)}$ concentration (b, acidic pH) at 450 °C, 1000 bar. Points correspond to experimental data (Table 1), lines were calculated using reaction constants from Table 2.

Fig. 3. Gold L_3-edge HERFD-XANES spectra of Au-bearing oxidized (experiments cap21, cap1), reduced (experiment cap 33) solutions, and model systems – solution of Au thiosulfate and $Au_2S_{(cr)}$. RT - room temperature. Vertical dashed lines indicate main features for Au in oxidized $Na_2S_2O_3$ solution at 350 °C/500 bar. Compositions of the experimental solutions are

given in Table 3 (1st row), and the solute speciation at the experimental *PT*-parameters is presented in Table A1.

Fig. 4. EXAFS spectra at Au L_3-edge (k^2 weighted) for experiments cap8 and cap21 (oxidizerd system), and their Fourier transforms (not corrected for phase shift) performed for different k – ranges. The S_L (HS^-), S_1 (S_3^-) – the nearest atoms to Au, S_2 – sulphur atom in the second coordination shell of Au.

Fig. 5. EXAFS spectra at Au L_3-edge: comparison of experimental spectra (oxidized system) with results of reverse Monte-Carlo simulations and spectra calculated using species geometries obtained by means of *ab initio* molecular dynamics. (a) experiment cap8. (b) experiment cap21. Fourier transforms are not corrected for phase shift. Results of AIMD simulations are given in Figures A2, A3, and A4.

Fig. 6. Results of Au L_3-edge HERFD-XANES spectra modeling. Calculations were performed using atomic configurations obtained from *ab initio* MD simulations. (a) cap33, reduced H_2S/NaOH fluid, 450 °C/500 bar. (b), (c), (d) cap21, oxidized $Na_2S_2O_3$ fluid, 350 °C/500 bar. The composition of Au complex for which the AIMD simulation was performed is indicated at the top of each figure. Energy scale is given relatively to the Fermi level.

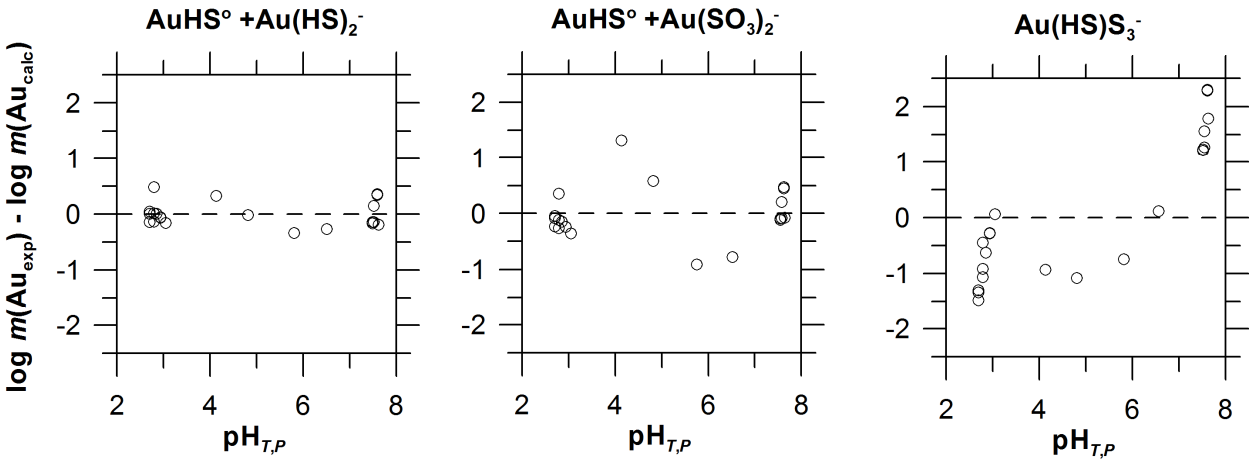
AuHS° +Au(HS)2-
AuHS° +Au(SO3)2-
Au(HS)S3-
log m(Auexp) - log m(Aucalc)
pHT,P
pHT,P
pHT,P

Figure 1

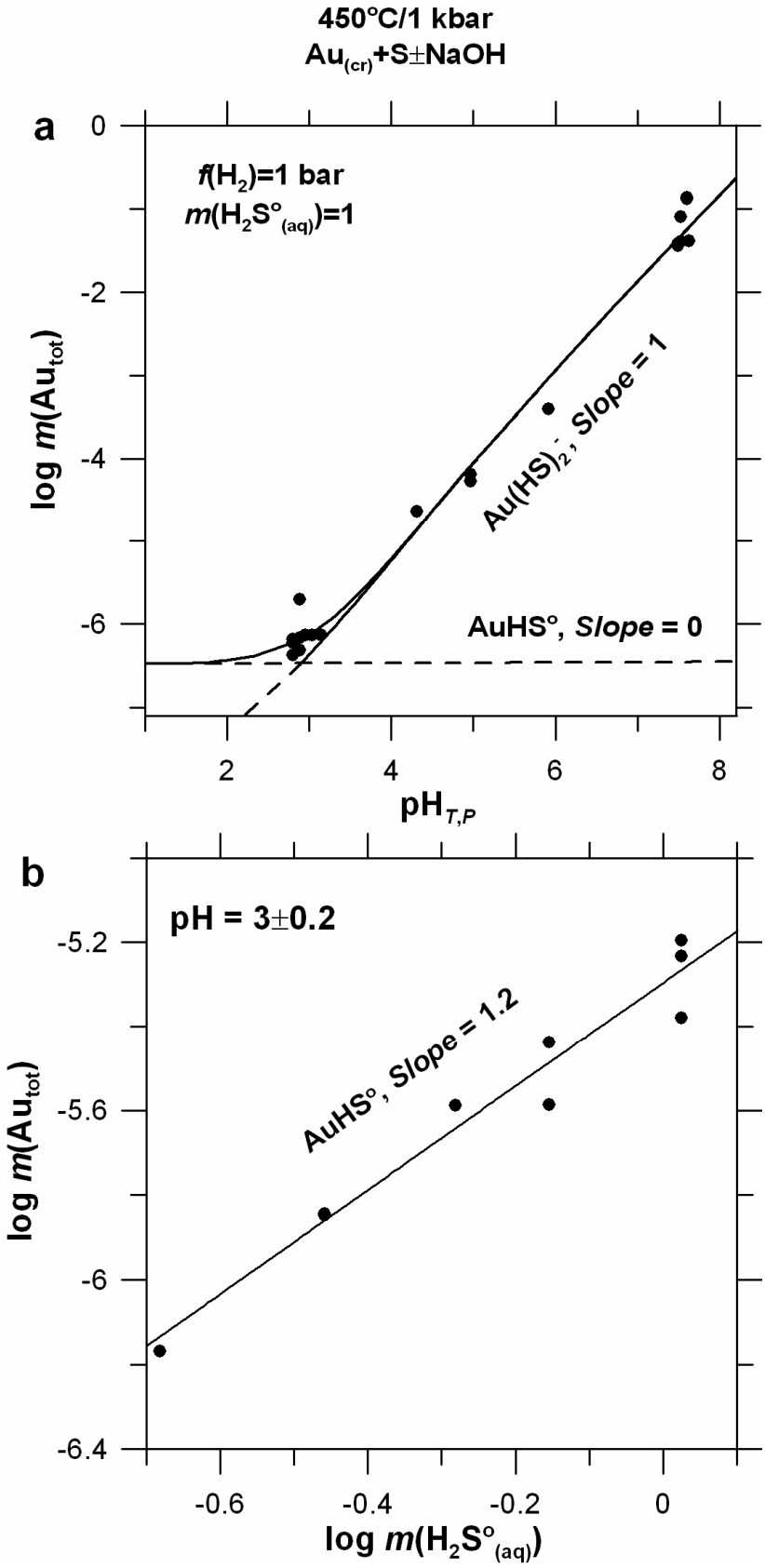
450°C/1 kbar
Au(cr)+S±NaOH
a
f(H2)=1 bar
m(H2S°(aq))=1
Au(HS)2-, Slope = 1
AuHS°, Slope = 0
log m(Autot)
pHT,P
b
pH = 3±0.2
AuHS°, Slope = 1.2
log m(Autot)
log m(H2S°(aq))

Figure 2

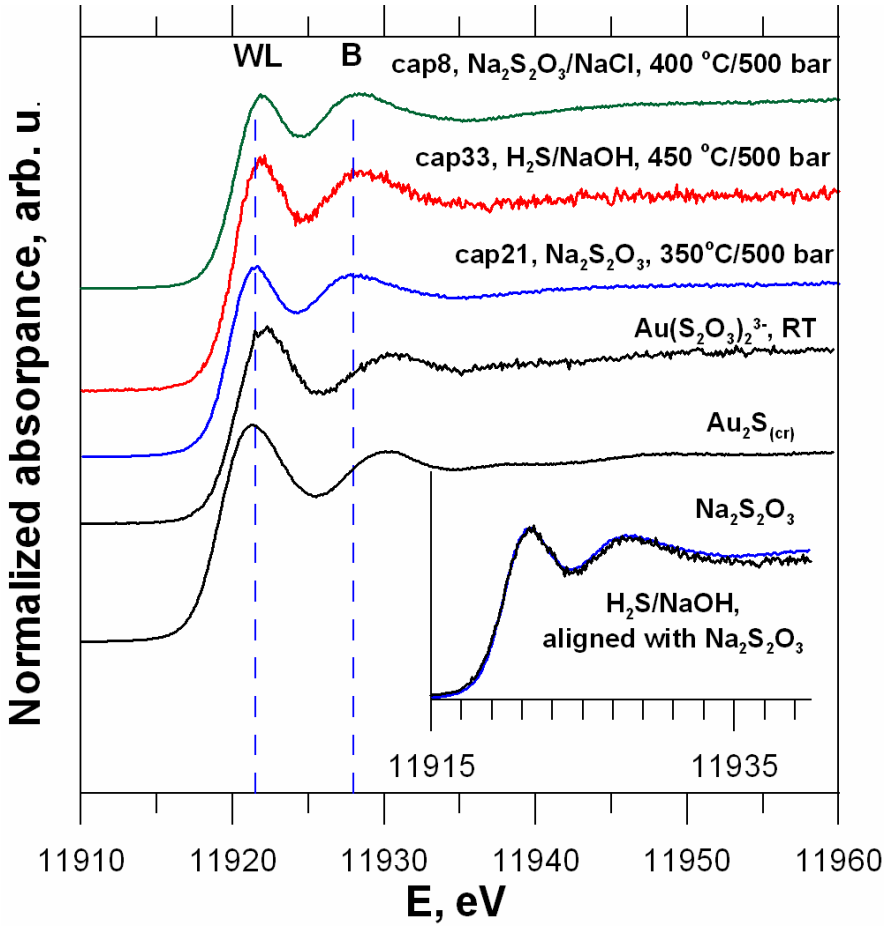
WL
B
cap8, Na2S2O3/NaCl, 400 °C/500 bar
cap33, H2S/NaOH, 450 °C/500 bar
cap21, Na2S2O3, 350°C/500 bar
Au(S2O3)2 3-, RT
Au2S(cr)
Na2S2O3
H2S/NaOH,
aligned with Na2S2O3
11915
11935
Normalized absorpance, arb. u.
11910
11920
11930
11940
11950
11960
E, eV

Figure 3

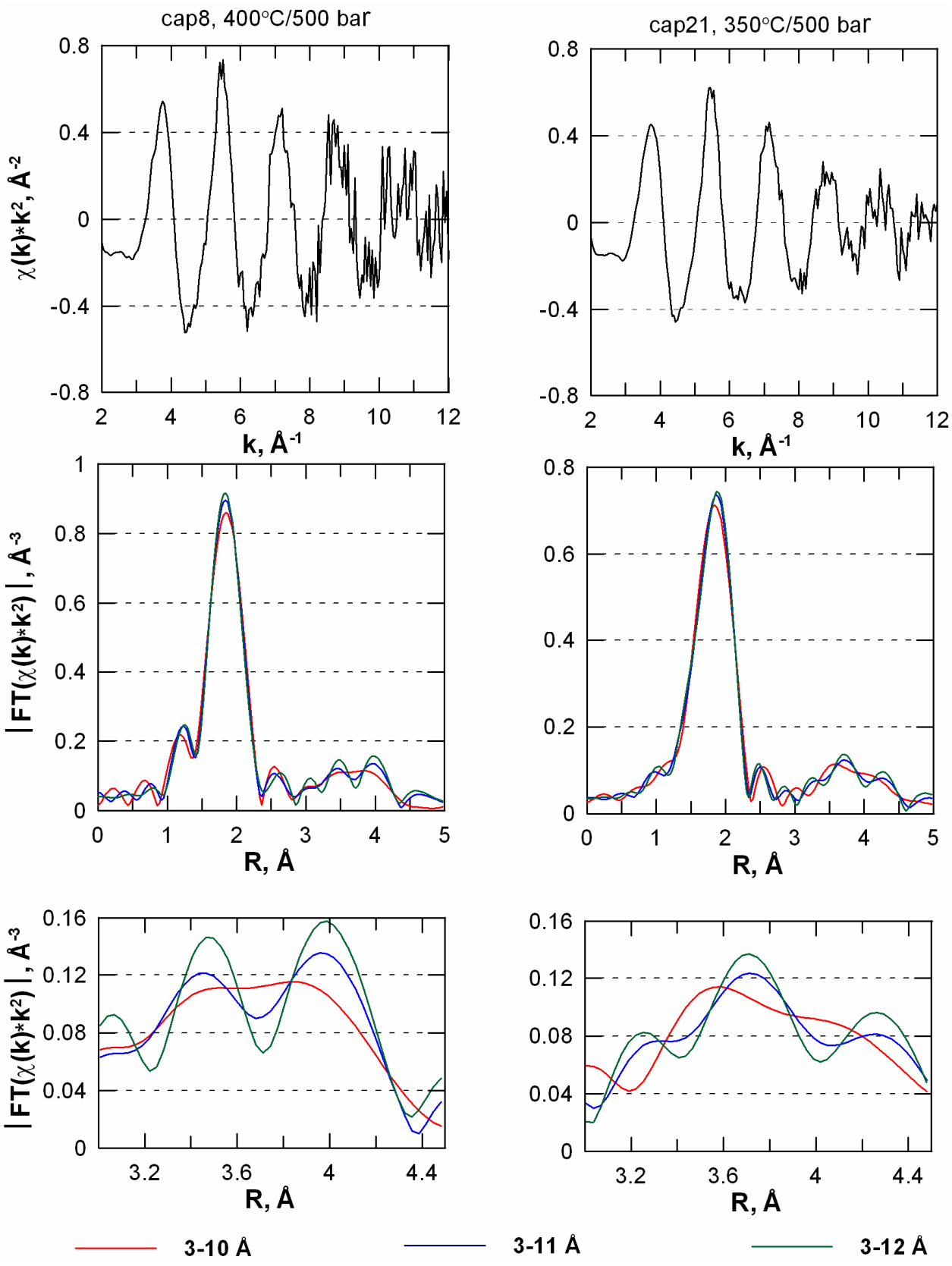
cap8, 400°C/500 bar
cap21, 350°C/500 bar
χ(k)*k², Å⁻²
k, Å⁻¹
|FT(χ(k)*k²)|, Å⁻³
R, Å
3-10 Å
3-11 Å
3-12 Å

Figure 4

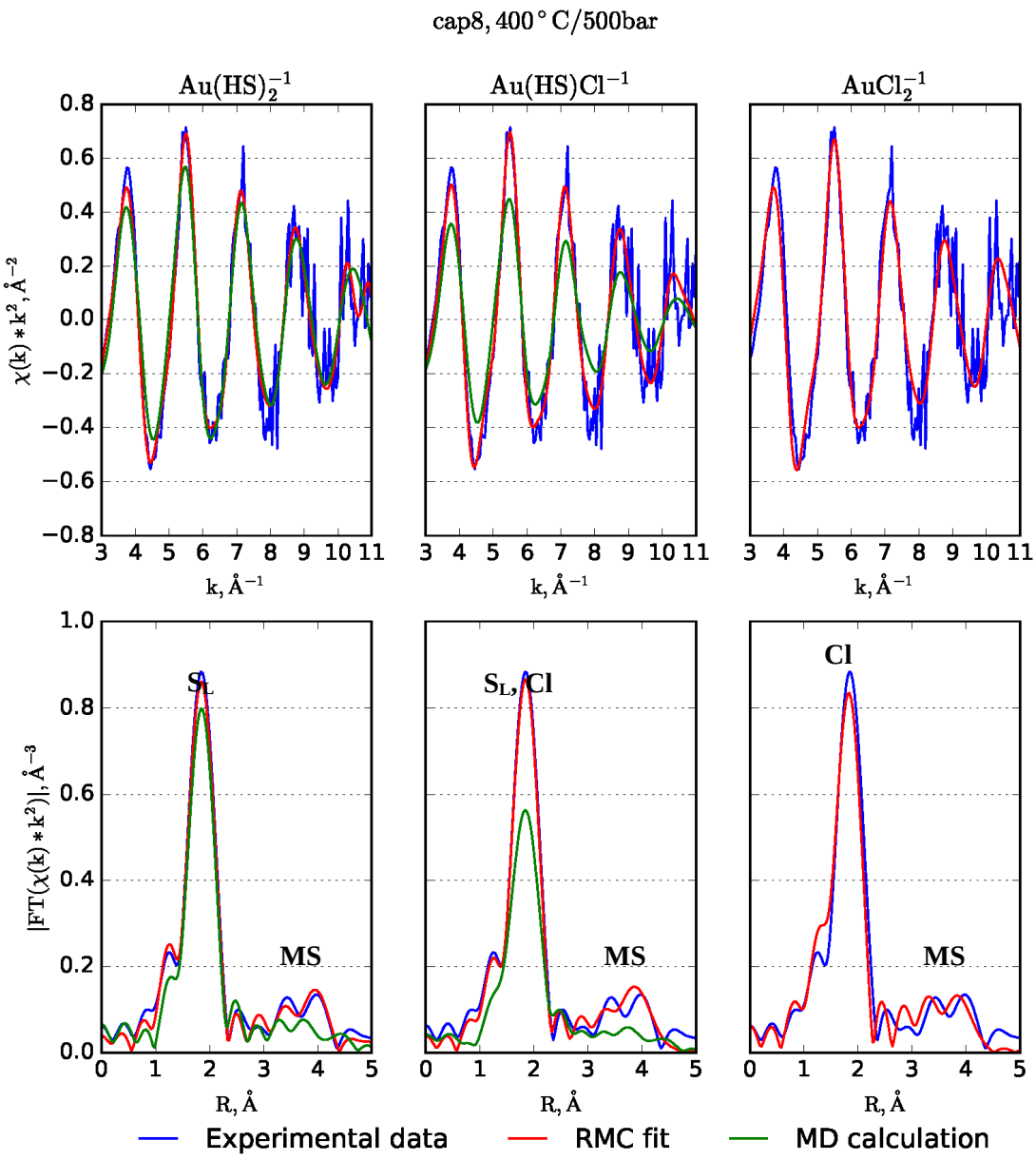
cap8, 400 ° C/500bar
Au(HS)$_2^{-1}$
Au(HS)Cl^{-1}
AuCl$_2^{-1}$
χ(k) * k^2, Å^{-2}
k, Å^{-1}
|FT(χ(k) * k^2)|, Å^{-3}
R, Å
S$_L$
S$_L$, Cl
Cl
MS
Experimental data
RMC fit
MD calculation

Figure 5a

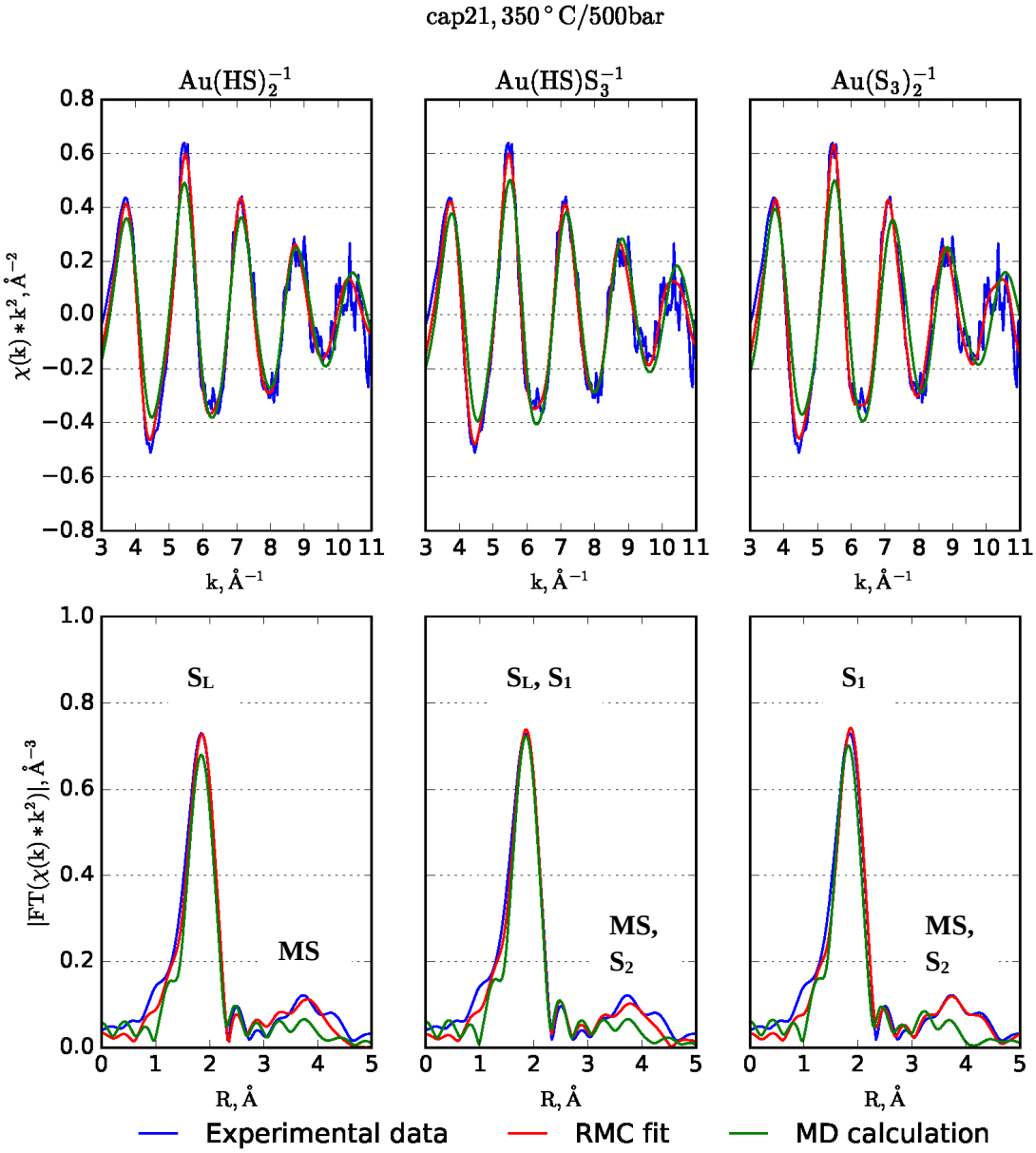
cap21, 350 ° C/500bar
Au(HS)$_2^{-1}$
Au(HS)S$_3^{-1}$
Au(S$_3$)$_2^{-1}$
χ(k) * k^2, Å^{-2}
k, Å^{-1}
|FT(χ(k) * k^2)|, Å^{-3}
R, Å
S$_L$
MS
S$_L$, S$_1$
MS, S$_2$
S$_1$
MS, S$_2$
Experimental data
RMC fit
MD calculation

Figure 5b

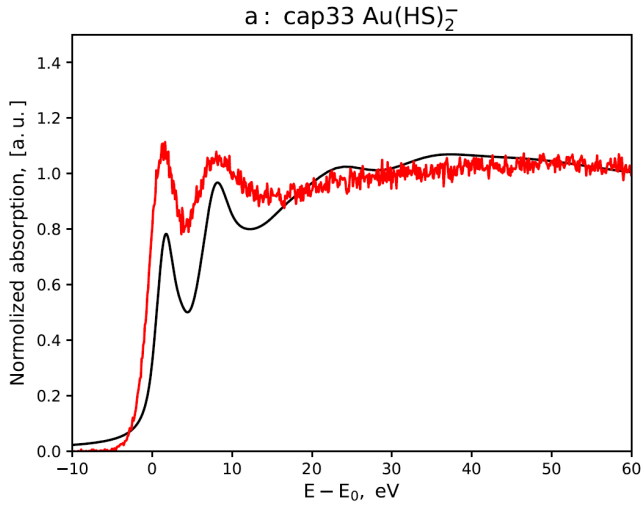
a : cap33 $Au(HS)_2^-$
Normolized absorption, [a. u.]
$E - E_0$, eV

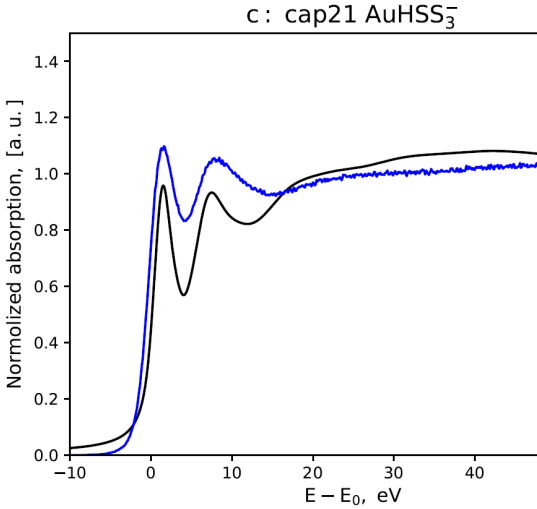
c : cap21 $AuHSS_3^-$
Normolized absorption, [a. u.]
$E - E_0$, eV

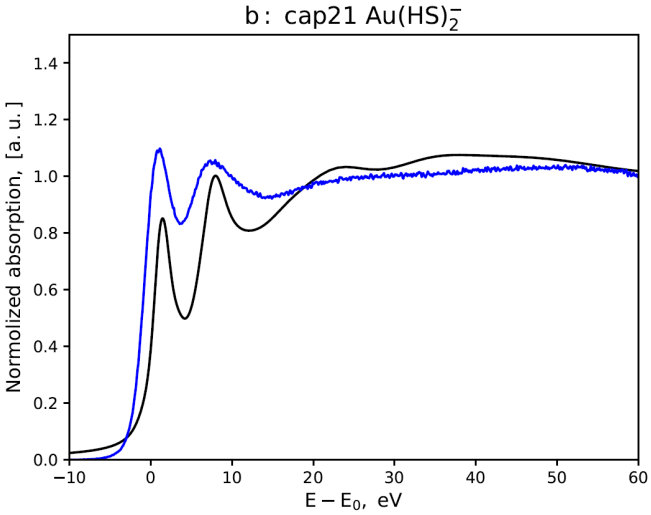
b : cap21 $Au(HS)_2^-$
Normolized absorption, [a. u.]
$E - E_0$, eV

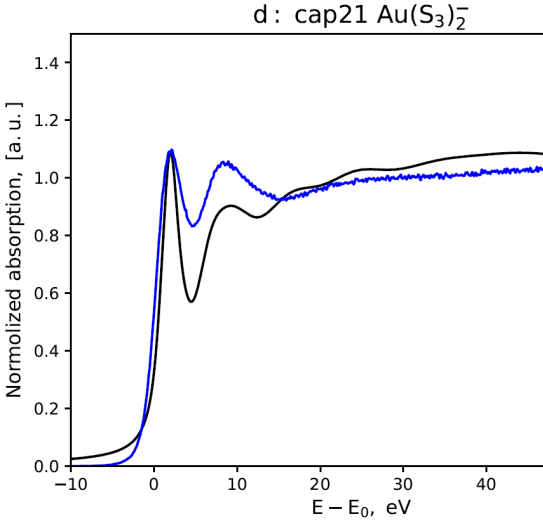
d : cap21 $Au(S_3)_2^-$
Normolized absorption, [a. u.]
$E - E_0$, eV